31st European Rotorcraft Forum - Florence, Italy, 13-15 September 2005 - Paper 109

Influence of wind-tunnel walls in helicopter aerodynamics predictions

M.Biava, J.-C. Boniface, L.Vigevano
Dipartimento di Ingegneria Aerospaziale, Politecnico di Milano, Italy

Abstract

Time-accurate numerical computations on a generic rotor-fuselage configuration are carried out by the ROSITA Euler code with the Chimera approach. The several body grids are embedded into a set of Cartesian background grids, automatically generated, which may account for the presence of wind tunnel walls. Preliminary computations have been successfully carried out, thus demonstrating the feasibility of the ROSITA solver in simulating rotor–fuselage interactions. Both free-flight and wind tunnel configurations are analyzed. However, the lack of trim data on the chosen hypothetical helicopter configuration prevented to select blade dynamics and fuselage pitch attitude such as to maximize the wall interference effects, that are demonstrated quite weak in the present case.

1 Introduction

The new generation of CFD codes being developed over the last decade are nowadays mature enough to simulate the flow field around complete helicopter configurations. Steady solutions of the Navier–Stokes equations [1] - [7] have been achieved with the actuator disk model, in which the rotor is replaced by an infinitely thin disk where source terms are introduced to represent the flow induced by the rotor itself. Many of these calculations make use of the Chimera overset grid technique to embed the actuator disk into a multi–block structured grid. The Chimera grid technique, naturally suited for describing multiple bodies in relative motion, has also been the key–point to allow for fully unsteady inviscid [8] - [10] and viscous [11],[12] rotor–fuselage calculations. A further advantage of the overset grid method is that it allows to ease the overall grid generation procedure, by subdividing a complex geometrical configuration into simpler components and generating independent body-fitted grids around each of the components. In this way the generation process of the grids defining solid bodies or part of solid bodies is strongly simplified.

The difficulty of the above approach – as far as grid generation is concerned – is shifted to the generation of the background grid, needed to assure the connectivity among the many body grids and to cover the whole computational domain. This may become particularly severe when the geometrical complexity increases, like for a rotor-fuselage configuration. It can be a very difficult task to generate manually a background grid with appropriate distribution of grid spacing such as to properly assure the connectivity among body grids of very different locations and cell sizes. Such a drawback has motivated the development of fully automatic procedures [13] – [16] for the generation of a system of overset (Chimera) background grids, that covers a given computational domain around an assigned number of body grids, while assuring correct connectivity properties.

Notwithstanding the achieved success, a meaningful validation of such CFD tools requires accurate experimental data, gathered with detailed wind tunnel testing. In the past, the experimental data were corrected in order to eliminate the interference effects of wind-tunnel walls and hence allowing to consider approximated free stream conditions [17]. Only in recent years, the numerical simulation of the wind-tunnel test has been recognized as a possible way of providing accurate boundary conditions to CFD codes, without requiring any kind of wall corrections.

In order to estimate the influence of the wall confinement on the predicted solution, some numerical computations have been carried out by on a generic rotor-fuselage configuration, with and without the presence of wind-tunnel walls. At this preliminary stage, the Euler solver ROSITA [18] has been used for the calculations, thus neglecting the viscous effects. The relative motion of the rotor blades is taken into account considering the Chimera approach, by generating body-conforming grids for each blade and for the fuselage, and embedding these grids into a composite system of cartesian background meshes (see Figure 1). The latter is produced automatically by a dedicated tool, which allows for the optional inclusion of the wind-tunnel walls directly into the background-grid system.

2 Solver description

The ROSITA solver numerically integrates the unsteady Euler equations, formulated in terms of absolute velocity and expressed in a rotating frame of reference RF linked to each blade. Additional source terms are introduced to apply the compressible vorticity confinement formulation [19]. The equations are discretized in space by means of a cell-centred finite-volume implementation of the Roe's scheme [20]. A high resolution scheme is obtained through the use of MUSCL extrapolation supplemented with a total variation diminishing (TVD) limiter to ensure monotone solutions. Time advancement is carried out with a dual-time formulation [21]. A 2^{nd} order backward differentiation formula was applied to approximate the time derivative and a fully unfactored implicit scheme is used in pseudo-time.

3 Grid generation

Either single- (for the blades) or multi-block (for the fuselage) grids are generated around the solid bodies considered. These *child* grids are complemented by a system of Chimera background grids. The proposed method follows the approach of Meakin [13],[14], in which the background discretization is made of topologically simple (hexahedral), uniform, overlapping Cartesian grids. Since each child grid may be specified into its own reference system, the rotation and translation matrices of each grid has also to be known. A single reference system, termed *Absolute Reference System* (ARS) has to be selected for the generation procedure: for instance, in the rotor-fuselage configuration presently considered, the fuselage reference system has been selected as ARS. The body grids are characterized by their spatial extent and location, defined through the coordinates of their bounding box in ARS. In case of relatively moving grids, the bounding box has to include all the spatial region covered by the body grid during its motion, i.e. it is formed by the union of all bounding boxes computed at different time steps during the motion.

The other important parameter derived from the child grids is the typical cell dimension S_b that characterizes their outer layers. To allow for proper overlapping between the body grids and the most fine background grids that embed them, the spacing of the fine background grids is assigned equal to S_b. All other background grids, that do not directly overlap with the body grids, are assigned a larger spacing, controlled by a derefinement criterium.

The fundamental tool of the method is the so-called phantom grid, an uniform, cartesian and rather coarse grid that covers the whole computational domain. Such a phantom grid is used to define a partitioning of the domain into separate spatial hexahedral blocks, that possess a one-to-one correspondence with the single grids forming the background system. To each cell of the phantom grid is associated a derefinement level indicator that drives the partitioning.

The problem of forming regular spatial blocks by coalescing phantom grid cells with equal derefinement level does not have a unique solution. Meakin suggested to sweep the phantom grid along coordinate lines [13] or to pass through the index space of the phantom grid with decreasing stride-lengths [14]. An alternative approach is suggested in [15], using dichotomic division and weakest descent merging [22]. In the present work a method has been developed that attempts to form blocks as much homogeneous as possible, i.e. with similar dimensions along the different coordinate lines. The method is based on a local search recursive procedure that forms the block by *growing* from an initial cell. Once the blocks are formed, a merging procedure try to minimize the number of blocks and the amount of block surface area.

The background grid generation procedure starts from the partitioning of the computational domain into blocks. Each grid has to cover a volume slightly larger than the corresponding block, to allow for grid overlap. Benoit and Jeanfaivre [15] state that overlaps of different extensions are needed between cartesian grids of different level of derefinement, in order to assure a correct connectivity. This problem is completely avoided in the present method by generating first a dual grid connecting the cell centers, that fully cover the corresponding block space. In this way the computational space is filled by *valid* internal points, that overlap at the interfaces between blocks, and each cell center grid may be extended of two layers in each direction, independently from the derefinement level of the neigh-

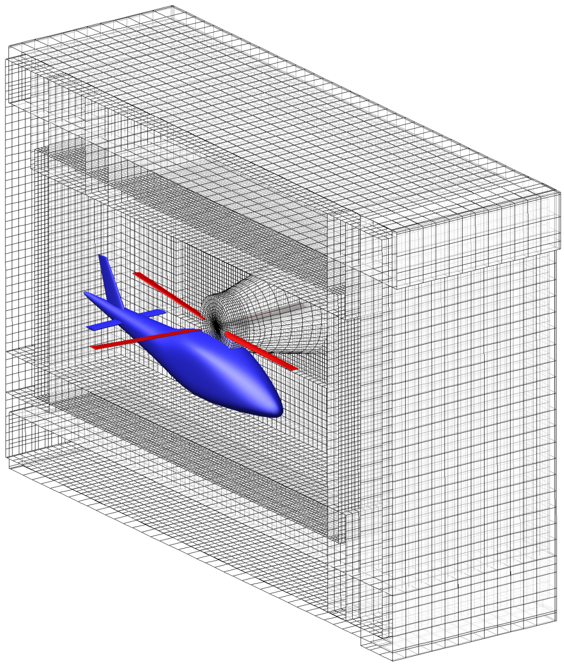

Figure 1: Helicopter configuration embedded in the system of cartesian background grids. One blade grid is also shown

boring blocks. Finally the background grid is easily recovered from the cell centers dual grid.

The last step of the procedure consists in computing the connectivity data among the different background grids. This is done once–and–for all for every background grids except the finest ones, that fully embed the child grids.

4 Description of test-cases

The considered rotor-fuselage configuration (Fig. 1) represents a possible helicopter model to be tested in a large scale wind tunnel test section. The model rotor, which diameter is 2.1 meters, is equipped with 7A blades while the fuselage geometry is similar to that used for the actual wind tunnel tests in the European project Heliflow.

In order to estimate the wind-tunnel wall effects, two computations have been carried out. A first reference computation, without wind-tunnel wall, aims at simulating free-flight conditions. Then a second computation has been performed taking into account the presence of the wind-tunnel walls, where solid-wall boundary conditions are applied. According to the presence of walls or not, as described hereafter, an appropriated space extent of the composite system of background grids must be considered.

Free-flight conditions are numerically reproduced considering the aircraft placed at the center of a composite system of cartesian background meshes extending away in a computational box with size of 13 x 9 x 9.5 rotor diameters in the free-stream, spanwise and normal directions respectively (see figure 2). Standard characteristic-like far-field conditions are applied at the outer boundaries. Undisturbed free-stream assumption is made outside of the background meshes.

The wind-tunnel simulation is achieved by defining the volume of the background meshes matching exactly with the dimensions of the wind-tunnel section of size 9.45x6x6 meters, as shown in figure 1. Wall interferences are reproduced by applying a slip condition to the test section ceiling, the lateral walls and the test section floor. A characteristic-like method has been imposed in order to simulate the inflow/outflow conditions at the upstream/downstrean cross-sections of the wind tunnel.

The hub geometry is not included in these preliminary calculations, nor is the model support. In the calculations considering the wall confinement, the rotor hub reference location, which represents the origin of the coordinate system used to specify the blade dynamics, is located at 4.2 meters from the inlet plane and 0.5 meters above the wind tunnel axis in the vertical symmetry plane.

Rotor dynamics and helicopter pitch were taken the same in both the constrained and free flow calculations. The advance ratio is $\nu = 0.214$ while the shaft angle is $\alpha = -2.5$ degrees. Since no trim data were available for this hypothetical configuration, the blade dynamics has been selected from previous isolated rotor calculations at the same aspect ratio value [18], notwithstanding that an inconsistency is introduced since the shaft angle is different in the present case.

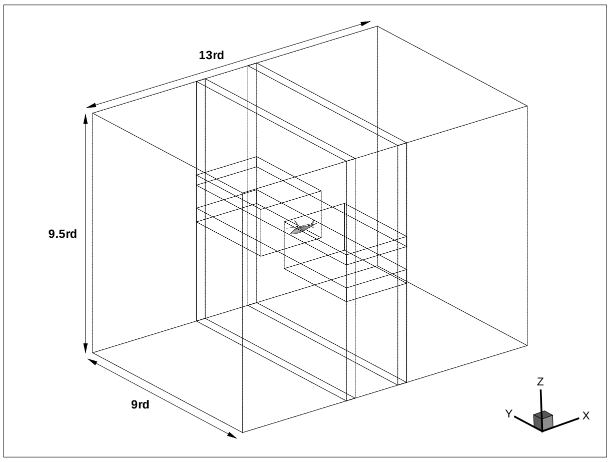

Figure 2: Extension of the cartesian background meshes for the free-flight simulation (in rotor diameters)

As mentioned earlier, the ROSITA solver operates in inviscid flow assumption for both computations. The grid generation is achieved within the procedure described above. In both cases, the automatic background-grid generation procedure starts from the same set of body-conforming grids. Regarding the four-bladed 7A rotor, single O-H grids have been generated around each blade with 60 (chordwise) x 53 (spanwise) x 25 (normal) grid points. The fuselage grid contains about 900 000 grid points in 19 blocks. These body-conforming grids are then complemented by a composite system of cartesian background grids generated automatically in order to fulfill the requirements of proper grid overlap and to ensure the prescribed spatial extent. The automatic grid generation procedure produces 1 350 000 grid points in 25 cartesian blocks for the free-flight simulation, and 1 250 000 grid points in 19 cartesian blocks when accounting for the wind-tunnel walls. All figures are summarized in table 1

The last step of the procedure consists in computing the grid tagging and interpolation coefficients required by the Chimera method among the different background grids. This is done once–and–for all for every background grids except the finest ones, that fully embed the rotating rotor-blade grids. The computation of the connectivity data corresponding to the rotating grids is performed first and are then passed to the flow solver as a set of input files, each corresponding to a specified azimuthal position of the rotor (typically for every one degree when using the dual-time stepping method).

	Fuselage	Rotor	Background	Total
Wind Tunnel	900000 (11 blocks)	318000	1250000 (19 blocks)	2468000
Free Flight	Identical	Identical	1350000 (25 blocks)	2368000

Table 1: Total number of grid points

Both computations have been performed in multiprocessor mode using 10 processors ATLON MP 1800. The computational time required for the grid-connectivity calculation and the flow solver after two rotor revolutions is reported in the table 2.

	Grid connectivity	Flow solver
Wind Tunnel	73 h	165 h
Free Flight	90 h	180 h

Table 2: CPU time in hours (multiprocessor mode)

5 Discussion of results

The results achieved in the free flight and wind-tunnel simulations are compared with the aim of observing the effects of the presence of close solid walls on the computed flow field and loads.

5.1 Flow field

The flow field computed for the two configurations is qualitatively very similar. As an example, the instantaneous streamlines are shown in figures 3 – 6.

The inclination of the rotor disk with respect to the free–stream direction is not high in the computed cases, nor is the total rotor thrust. As a consequence the flow is only slightly deviated from its main direction and the effects of the wall confinement is not very relevant. This is confirmed by the analysis of the vorticity field, depicted in Fig. 7 only for the wind tunnel case, being the other very similar. It can be observed how the rotor wake is deviated in downwards direction only in its inner

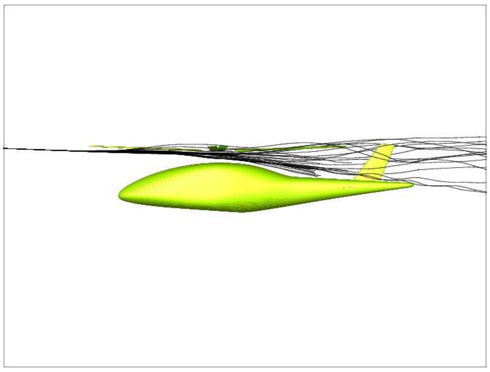

Figure 3: Side view of streamlines – free flight case

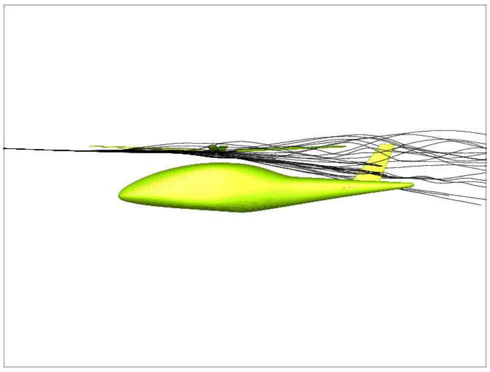

Figure 4: Side view of streamlines – wind tunnel case

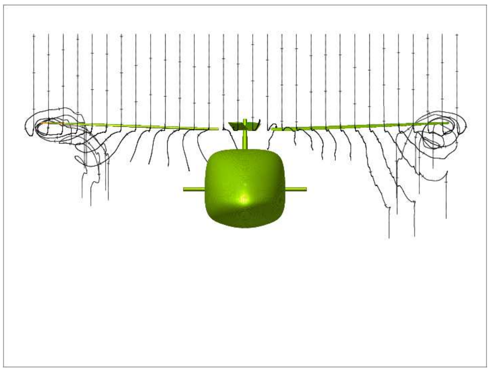

Figure 5: Front view of streamlines – free flight case

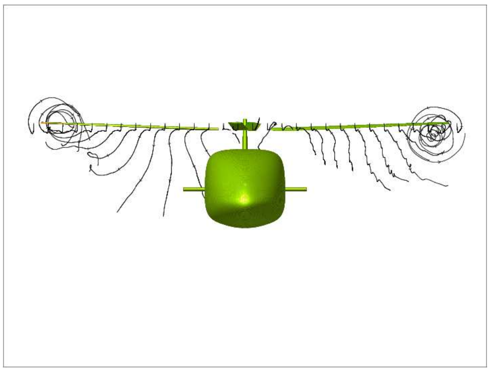

Figure 6: Front view of streamlines – wind tunnel case

portion, while most of the tip vortex vorticity is coalescing into two streamwise vortices that retain the free–stream direction.

The fact that the flow into the wind tunnel is only slightly perturbed by the rotor wake in the present case is also confirmed by the observation of the instantaneous pressure distribution on the tunnel lower and upper walls, Fig. 8. The wall pressure fields are not uniform but the magnitude of the disturbances is very limited.

5.2 Blade loads

A quantitative appraisal of the influence of the wall confinement on the rotor loads may be appreciated looking at the variation of the normal force coefficient on one blade during one period of revolution (Fig.9). The shape of the azimuthal load distribution is not altered by the presence of the tunnel walls, that only gives rise to a slight increase of the value of the normal force coefficient itself, more pronounced for the advancing blade.

5.3 Fuselage loads

The azimuthal distribution of the integrated normal force coefficient over the fuselage and tail planes is shown in Fig. 10, where we can observe that the low pitch angle of the fuselage gives rise to low loads. Therefore is such conditions the slight difference between the two test cases is expected and the phase difference observed in Fig. 10 not particularly significant. Also the instantaneous surface pressure distributions depicted in figures 11 and 12 do not differ significantly, thus leading to very similar time-integrated distributions (Figures 13 and 14).

6 Conclusions

Numerical computations on a generic rotor-fuselage configuration carried out by the ROSITA code demonstrate that an unsteady CFD analysis of the complex helicopter flow field is feasible, although computationally expensive. The simulations were aimed at assessing the influence of the presence of wind-tunnel walls on the rotor and fuselage loads.

Unfortunately, the lack of trim data on the chosen hypothetical helicopter configuration prevented to select the blade dynamics and fuselage pitch attitude such as to maximize the wall interference effects, that have been demonstrated quite weak in the present case. Further simulations on more realistic trimmed configurations and additional validation against experimental data are required to substantiate the ansatz that time-accurate CFD analysis may become a useful tool to extrapolate reduced-scale wind tunnel results into full-scale conditions.

Acknowledgements

This work has been partly supported by Agusta under the contract 01/172/VIL.

References

[1] Zori L., Rajagopalan G. (1992). Navier–Stokes Calculations of Rotor–Airframe Interaction in Forward Flight, 48th Annual Forum of the American Helicopter Society, Washington, DC.

[2] Duque E.P.N., Dimanlig A.C.B. (1994). Navier–Stokes Simulation of the AH–66 (Comanche) Helicopter, Proceedings of American Helicopter Society Aeromechanics Specialists Conference for Aerodynamics, Acoustics and Dynamics, S.Francisco, CA, paper 3.7, 1–15.

[3] Bettschart N. (1999). Rotor fuselage interaction: Euler and Navier–Stokes computations with an actuator disk, 55th Annual Forum of the American Helicopter Society, Montreal, Canada.

[4] Brezillon J. (2000). Simulation of Rotor–Fuselage Interactions by using an Actuator Disk, 26th European Rotorcraft Forum, The Hague, Netherlands.

[5] Sidès J., Pahlke K., Costes M. (2001). Numerical simulation of flows around helicopters at DLR and ONERA, *Aerosp. Sci. Technol.*, **5**, 35-53.

[6] D'Alascio A., Berthe A., Le Chuiton F. (2003). Application of CFD to the fuselage aerodynamics of the EC145 helicopter. Prediction of unsteady phenomena and of the time averaged influence of the main rotor, 29th European Rotorcraft Forum, Friedrichshafen, Germany.

[7] Renaud T., Benoit C., Boniface J.-C., Gardarein P. (2003). Navier–Stokes Computations of a Complete Helicopter Configuration Accounting for Main and Tail Rotors Effects, 29th European Rotorcraft Forum, Friedrichshafen, Germany.

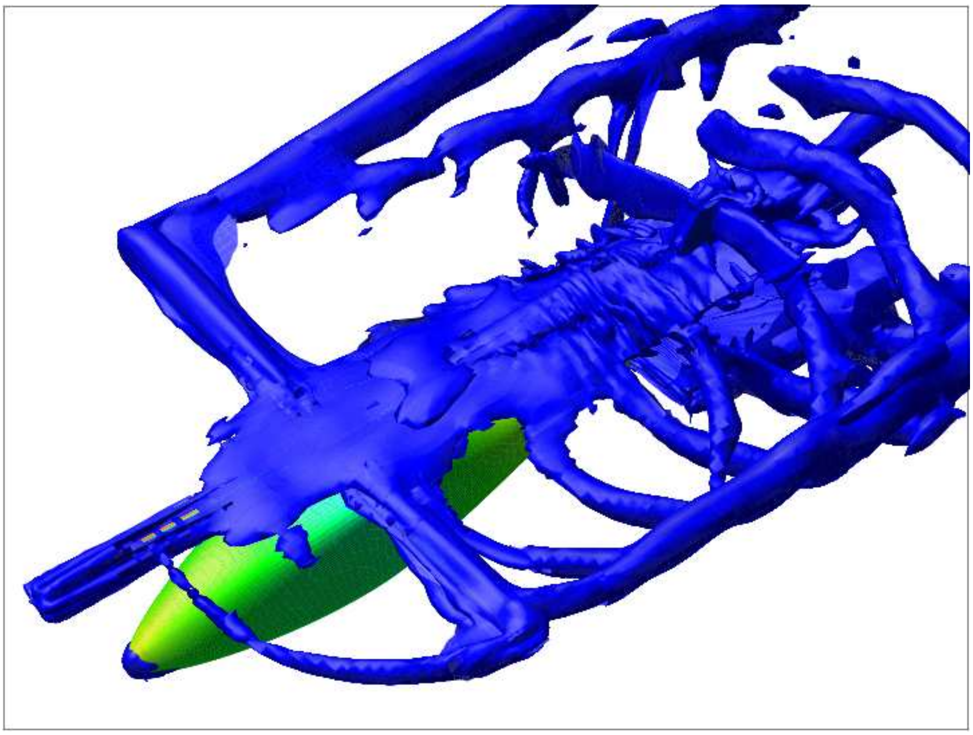

Figure 7: Vorticity field

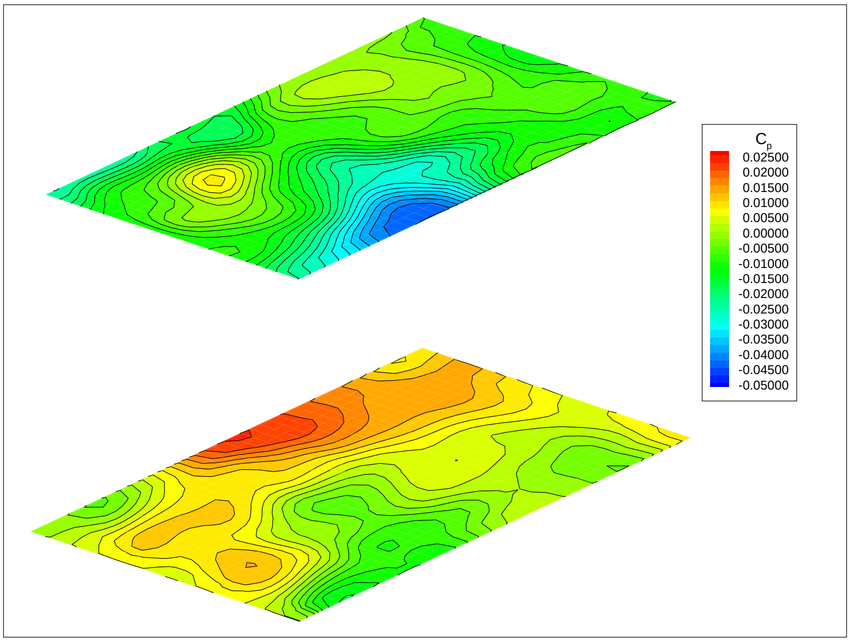

Figure 8: Instantaneous pressure distribution wind tunnel lower and upper walls

[8] Stangl R., Wagner S. (1996). Euler Simulations of a Helicopter Configuration in Forward Flight Using a Chimera Technique, 52nd American Helicopter Society Annual Forum, Washington, DC.

[9] Boniface J.-C., Guillen P., Le Pape M.C., Darraq D., Beaumier P. (1998). Development of a Chimera Unsteady Method for the Numerical Simulation of Rotorcraft Flow–fields, 36th ASME, Reno, NV, AIAA Paper 98–0421.

[10] Hariharan N., Sankar L.N. (2003). Unsteady Overset Simulation of Rotor–Airframe Interaction, *J. of Aircraft*, **40**, 662-674.

[11] Meakin R.L. (1993). Moving Body Overset

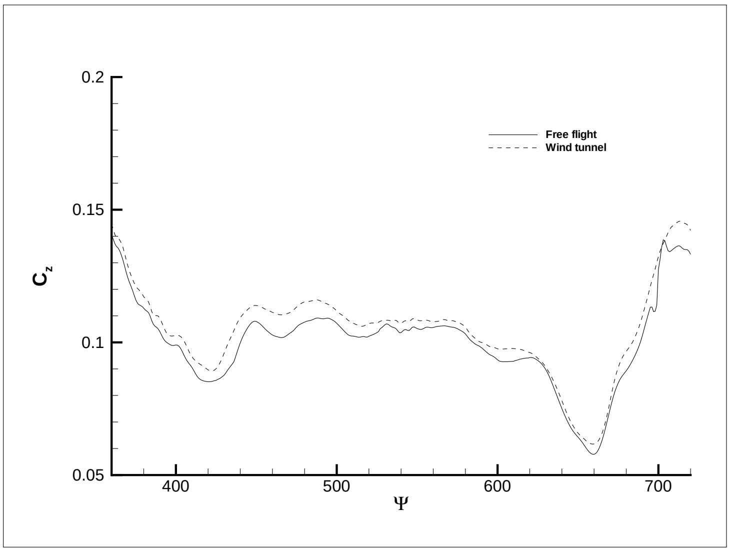

Figure 9: Blade loads in one revolution period

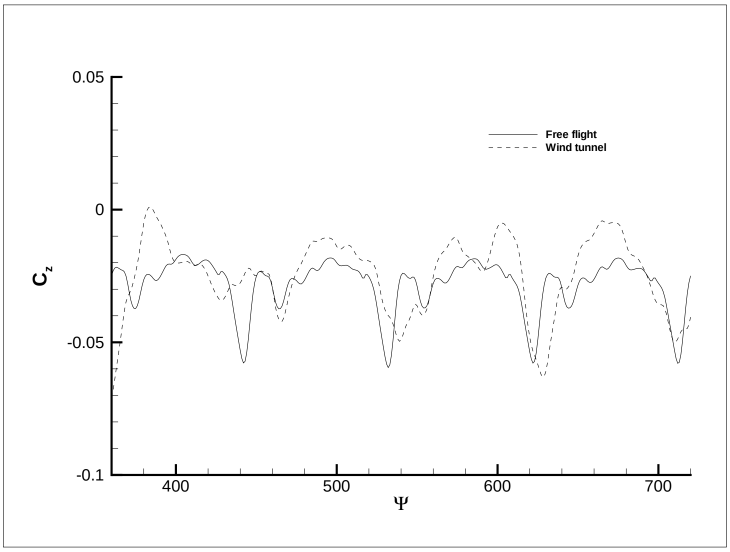

Figure 10: Fuselage loads in one revolution period

Grid Methods for Complete Aircraft Tiltrotor Simulations, 11th AIAA Computational Fluid Dynamics Conference, Orlando, FL, AIAA 93-3350.

[12] Khier W., Le Chuiton F., Schwarz T. (2002). Navier–Stokes Analysis of the Rotor–Fuselage Interference in Forward Flight. CEAS Aerospace Aerodynamics Research Conference, Cambridge, UK.

[13] Meakin R.L. (1995). An Efficient Means of Adaptive Refinement Within Systems of Overset Grids, AIAA Paper 95–1722–CP, 844-857.

[14] Meakin R.L. (2000). Adaptive spatial partitioning and refinement for overset structured grids, *Comput. Methods Appl. Mech. Eng.*, **189**, 1077-1117.

[15] Benoit C., Jeanfaivre J. (2003). Three–Dimensional Inviscid Isolated Rotor Calculations Using Chimera and Automatic Cartesian Partitioning Methods, *J. of the American Helicopter Society*, **48**, 128-138.

[16] Khier W., Schwarz T. (2003). Application of Cartesian Background Grid in combination with Chimera Method to predict Aerodynamics of Helicopter Fuselage, 29th European Rotorcraft Forum, Friedrichshafen, Germany.

[17] Langer H.-J. (1996). An experimental evaluation of wind tunnel wall correction methods

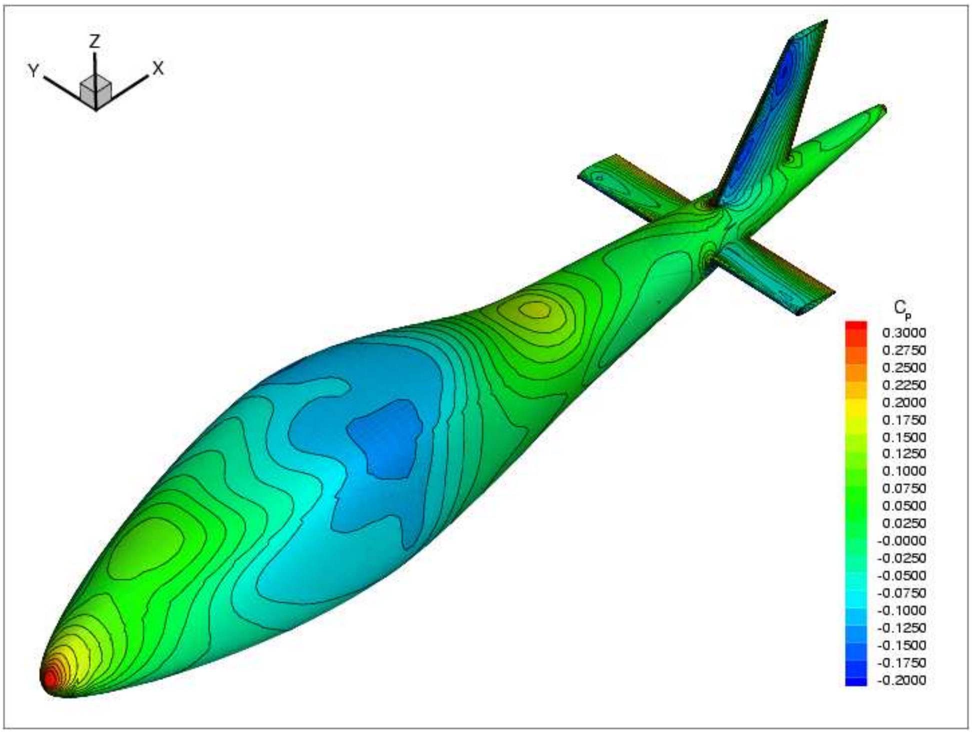

Figure 11: Instantaneous pressure distribution on the fuselage - free flight case

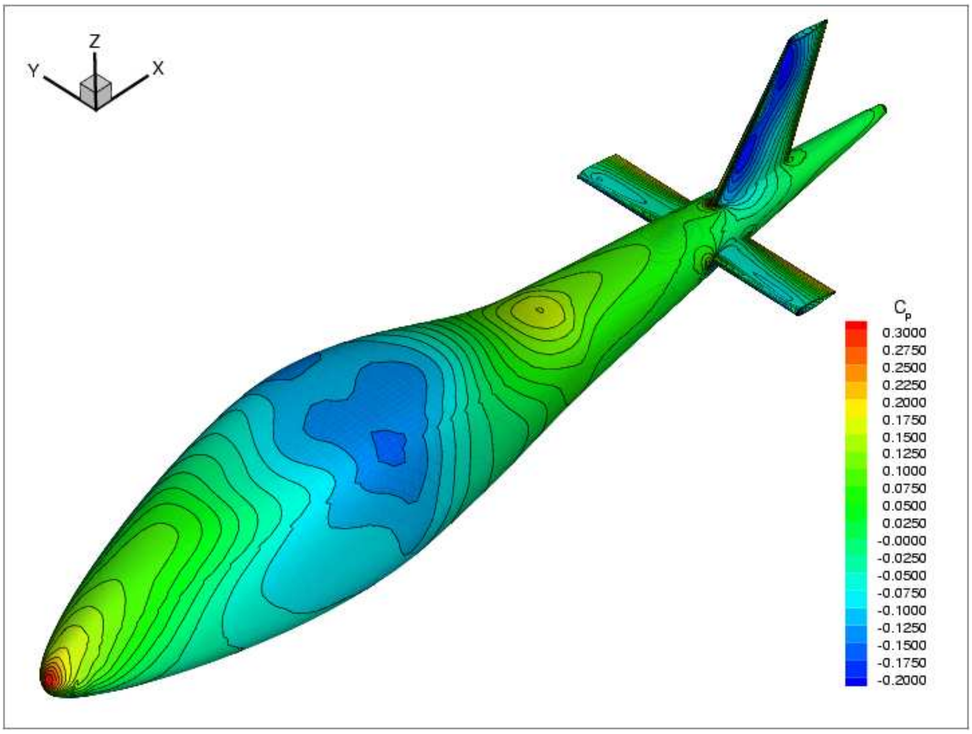

Figure 12: Instantaneous pressure distribution on the fuselage - wind tunnel case

for helicopter performance, 52^{nd} American Helicopter Society Annual Forum, Washington, DC.

[18] M. Biava, A. Pisoni, A. Saporiti, L. Vigevano. Efficient rotor aerodynamics predictions with an Euler method, 29^{th} European Rotorcraft Forum, Friedrichshafen, Germany, 16-18 September 2003.

[19] Biava M., Vigevano L. (2003). Assessment of the vorticity confinement technique applied to

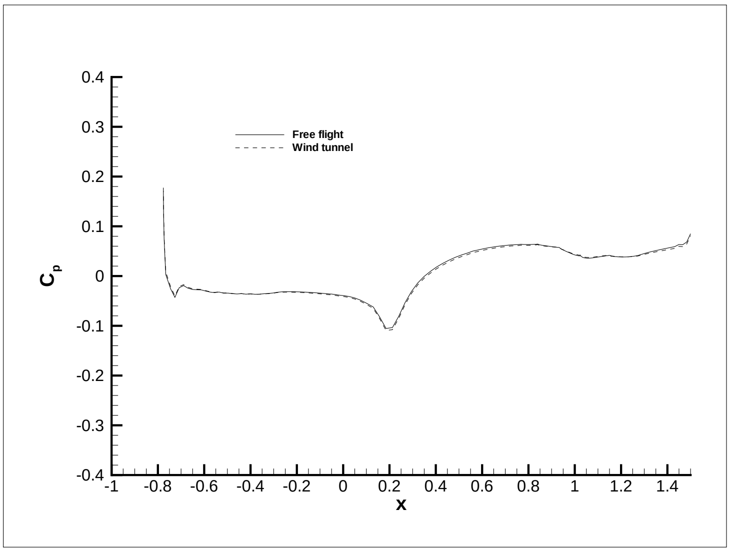

Figure 13: Time-integrated pressure distribution on fuselage symmetry plane - lower side

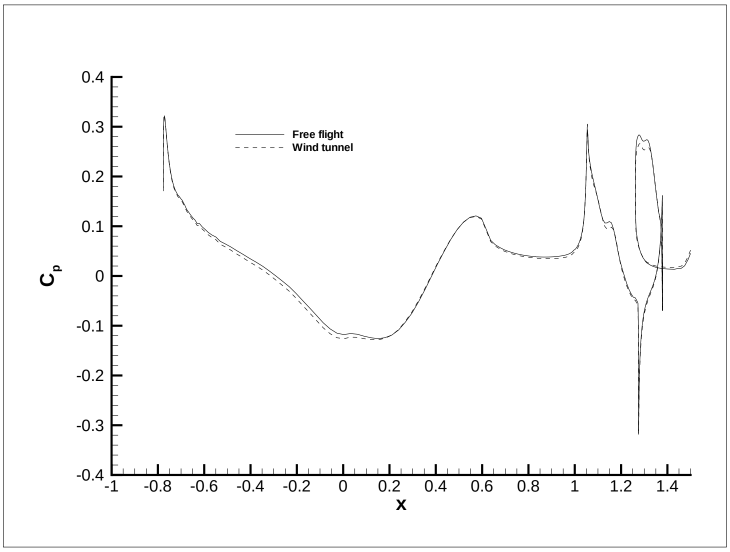

Figure 14: Time-integrated pressure distribution on fuselage symmetry plane - upper side

rotorcraft flows, 21^{st} AIAA Applied Aerodynamics Conference, Orlando, FL, AIAA 2003-3524.

[20] Roe P.L. (1981). Approximate Riemann Solvers, Parameter Vectors and Difference Schemes, *Journal of Computational Physics*, **43**, 357-372.

[21] Jameson A. (1991). Time Dependent Calculations Using Multigrid with Applications to Unsteady Flows past Airfoils and Wings, 10^{th} AIAA Computational Fluid Dynamics Conference, Honolulu, HI, AIAA 91-1596.

[22] Rigby D. L. (1996). Method of Weakest Descent for Automatic Block Merging, 15^{th} International Conference on Numerical methods in Fluid Dynamics, Lecture Notes in Physics, Springer, 522-527.